Large-area irradiance-mode spectral response measurements of solar cells by a light-emitting, diode-based integrating sphere source

Behrang H. Hamadani, John Roller, Andrew M. Shore, Brian Dougherty, and Howard W. Yoon

Note: This work has been published online with the following citation:

The final journal-formatted version can be found at:

The version shown below is the final NIST-approved unformatted manuscript and is provided for the general public for informational purposes.

Large-area irradiance-mode spectral response measurements of solar cells by a light-emitting-diode-based integrating sphere source

Behrang H. Hamadani,[1,*] John Roller,[1] Andrew M. Shore,[1] Brian Dougherty[1], and Howard W Yoon[2]

[1]*Engineering Laboratory, National Institute of Standards and Technology, Gaithersburg, MD 20899, USA*
[3] *Physical Measurements Laboratory, National Institute of Standards and Technology, Gaithersburg, MD 20899, USA*

[*]*behrang.hamadani@nist.gov*

Abstract: An irradiance-mode absolute differential spectral response measurement system based on a light emitting diode (LED) array is described. The LEDs are coupled to an integrating sphere whose output irradiance is uniform to better than 2 % over an area of 160 mm by 160 mm. Spectral response (SR) measurements of solar cells when subject to diffuse irradiation, as provided by the integrating sphere, are compared with collimated irradiance SR measurements. Issues originating from the differences in angular response of the reference versus the test cells are also investigated.   The spectral response curves of large-area cells with dimensions of up to 155 mm are measured and then used to calculate the cell's short circuit current (I_{sc}), if illuminated by a defined solar spectrum. The resulting values of I_{sc} agree well with the values obtained from secondary measurements.

1. Introduction

Irradiance-mode spectral response (SR) measurements of solar cells [1], which should be performed under uniform overfilled illumination and proper light biasing, can be used to predict the short circuit current (I_{sc}) of photovoltaic (PV) cells under any incident spectral irradiance, including the standard air mass 1.5 (AM 1.5) solar spectrum [2–4]. The differential SR method is the most common way of performing spectral response measurements of solar cells [3–10]. In this technique, a small modulated (quasi) monochromatic light beam and a steady-state bias light simultaneously illuminate the solar cell, producing a photocurrent that corresponds to the sum of these two sources: a small pulsed current signal superimposed on a (typically) larger direct-current (dc) current. The pulsed portion of the cell's output current is separated, amplified and detected by a lock-in amplifier that is synchronized with the user-selected modulation frequency of the monochromatic source. At the same time, a small portion of the modulated monochromatic light is split off and directed to a calibrated detector whose scaled output provides a measurement of the source's incident power (or irradiance) at the test plane. This measurement by the calibrated detector is either performed concurrently with the cell's photocurrent measurement, or shortly thereafter, with both measurements being coupled with the known wavelength of the modulated incident source. Collectively, the three values – modulated source's wavelength, calibrated detector output, and test cell photocurrent – define a discrete SR data point. The set of these discrete points, over the spectral range where the device is responsive to the incident radiation, construct the overall SR curve.

LEDs have been recently used as alternative (quasi)monochromatic light sources for spectral response and quantum efficiency (QE) measurements [11–14], and as broad band sources for

solar simulators [11,15,16], as well as being applied in other related applications [17,18]. Previously at NIST, two complementary techniques using LEDs were developed that yielded reasonably good SR data on small-sized solar cells [12]. For this prior work, the LED array of the differential SR measurement system was coupled to the inlet of a tapered optical waveguide. The prototype system, however, suffered from sources of error that resulted in unsatisfactory uncertainties in the measured spectral responsivities. The most significant sources of uncertainty were related to the non-uniformity of the illumination at the test plane and the lack of a concurrent irradiance measurement while the device undergoing testing was illuminated. The nonuniformities of the illumination resulted in patterns of "hot" and "cold" spots, with changes as high as 10 % or more over distances of a few centimeters. This non-uniformity introduced a proportionally larger source of measurement uncertainty in the SR curve for larger area solar cells. Also, the LED irradiances were not simultaneously monitored and so instead a substitution method was used. For this application, substitution was not sufficiently effective because the intensity and spatial distribution of the illumination drifted between the calibration step, with the calibrated detector in the test plane, and the subsequent measurements step with the device under test (DUT) installed in the test plane. Finally, on a practical implementation basis, the original approach was not preferred due to the very large size of the light guide (5 m long), which occupied a significant amount of lab space. By comparison, the new approach described in this paper uses an integrating sphere-based, LED-coupled light source that produces an extremely uniform illumination plane, while providing simultaneous irradiance monitoring. As a consequence, the measurement uncertainties in cell I_{sc} values have been substantially reduced, to generally less than 0.8 % (k=2) for small area (2 cm × 2 cm) single-junction cells and 1.2 % (k=2) for cells up to 15 cm × 15 cm.

The new LED integrating sphere measurement approach offers a robust method for ultimately calculating the short circuit current of a solar cell (when subject to any specified solar spectrum). To most easily make this calculation and avoid complications associated with accurately measuring the active area of a cell and/or trying to account for any cell non-uniformities, the irradiance-mode SR curve of the cell must be determined. For the new approach, moreover, only irradiance-mode measurements are made. By comparison, the approach previously taken was to first use a monochromator system to generate the cell's power-mode SR curve. This power mode SR curve was then converted to an irradiance mode SR curve by scaling the former using results from a single irradiance-mode SR measurement where only one LED was used to overfill the cell [10]. Power-mode measurements are conducted by having the monochromatic beam underfill the cell; such measurements require the knowledge of the monochromatic beam's radiant power, which is typically obtained using a calibrated, SI-traceable reference photodetector. In contrast, for irradiance-mode SR measurements, the monochromatic source overfills the solar cell and measurement of the irradiance or incident power per unit area of the source is required. Although both the previous and new approaches work well for small reference cells with relatively uniform material compositions, the single LED scaling method has limitations when used for solar cells having a varying spectral response behavior across the cell's total surface area. The LED integrating sphere approach avoids this limitation. In short, using only overfill measurements that provide an overall average irradiance-mode SR curve are superior to SR curves that can't easily account for the effects of cell non-uniformities, including the effects of front contacts. A few specific examples are provided in this paper to show the relative benefits of the new LED integrating sphere approach.

2. Measurement system characterization

A. Overall system description

Figures 1(a) and 1(b) show the schematics of the National Institute of Standards and Technology (NIST) LED-based spectral response measurement system using a custom integrating sphere. The sphere has a diameter of 50.8 cm (20 in) and a 12.7 cm (5 in) rear port for incorporating an LED-array plate of 11 cm by 11 cm. This array includes 33 LEDs ranging in wavelength from 373 nm to 1193 nm. The sphere has a exit port having a diameter of 22.9 cm (9 in). Port reducers of various sizes are available to allow size options for the exit port opening. A center baffle placed $\approx$ 16.8 cm (6.6 in) away from the rear port blocks the line of sight between the input and exit ports, thus promoting a more uniform illumination at the exit. Four additional 2.5 cm (1 in) ports are built into the sphere at locations around the exit port and each is equipped with a baffle. These 2.5 cm ports are used for adding dc light bias sources. Finally, two 1.3 cm (0.5 in) ports, which are also located near the sphere's exit port, accommodate the attachment of one monitor silicon (Si) and one monitor germanium (Ge) detector. The inner surface coating of the sphere, including all the baffles and port reducers, is a special barium sulfate formulation that has a very high diffuse reflectivity (96 % - 98 % at 600 nm) and good thermal stability to $\approx$ 373 K. The sphere and all attached parts are supported by a custom metal frame and opto-mechanical components.

The 33 pulsed LEDs and the four light bias LEDs are all mounted on water-cooled plates with the water temperature set at 288 K (15 °C). The pulsed LEDs are powered by computer-controlled LED drivers that regulate the current supplied to each LED. A function generator sequentially triggers each LED driver to apply a pulsed current to a corresponding LED at a user-selected frequency (typically less than 100 Hz, no multiples of 60 Hz). At the same time, very stable dc power sources supply constant voltages to the combination of visible and infrared light bias LEDs. The generated photocurrent from the solar cell, which is placed either directly at the exit port location or further back, is input to a variable-gain transimpedance current-to-voltage preamplifier that separates the photocurrent into its steady-state and pulsed components. This custom preamplifier is capable of handling up to 1.6 A of dc current. The ac cell signal is fed to an analog-signal switchbox. Furthermore, the signals collected by both the Si and the Ge detectors are input to a current-to-voltage amplifier and the voltage output from both of these amplifiers are fed to two input channels of the switchbox. The output of the switchbox, which can sequentially connect all 3 incoming signals, is input to a lock-in amplifier. For each LED measurement, the cell's signal followed immediately by either the Si or Ge detector's signal (depending on the illumination wavelength) is measured by the lock-in amplifier and recorded by the computer. Although the cell and the detector signals are not recorded simultaneously, they are nonetheless measured over a very short time interval (within a few seconds) and the LED output during this time interval is very stable. Also, a series of a few data points are collected for each different LED setting to aid the statistical analysis.

Cell illumination and measurements were performed in two different configurations. In configuration 1 (Fig. 1a), the cell is mounted directly at the plane of the exit port. Therefore, the device is exposed to a very diffuse light for both the pulsed and the steady bias illumination. This location may not necessarily cause any issues in the spectral response measurements unless the reference cell or detector – which is used for transfer of the irradiance scale to the Si and Ge monitor detectors – has an angular responsivity that is sufficiently different from the cell undergoing testing. Many different types of reference cells that were tested in our laboratory did indeed show non-ideal cosine behavior, particularly at incident illumination angles greater than 30°. Therefore, the transfer of the irradiance scale from a reference detector that was calibrated under normal incident illumination to cells measured with diffuse light would introduce a substantial error in spectral response of the cell due to the angular mismatch. To understand and correct for this effect, configuration 2 (Fig. 1b) was designed where the exit port was reduced to a 5.08 cm (2 in) port and an optics

assembly was mounted onto the port to project more collimated light from the sphere. In this case, the cell was mounted 60 cm from the sphere's exit port; the cell remained fully illuminated by the sphere's projected light. For this offset configuration, additional sources of bias light were installed on either side of the cell to off-axially illuminate the entire active (and inactive) areas of the test cell. Even in configuration 2, the pulsed optical power was sufficiently intense to perform the measurements with very good stability and reproducibility.

B. The LED array

The LED array consists of 33 monochromatic LEDs with wavelengths ranging from 373 nm to 1193 nm. The magnitude of the supplied LED currents can range anywhere from 1 mA to a few hundred mA. The center emission wavelength for some of the LEDs can change depending on the applied current. Of these LEDs, some shift by as much as 9 nm while the others shift between 1 nm and 3 nm. Due to this variation, the center wavelength for each applied current setting should be determined separately. (It has been observed, moreover, that at higher current settings, the intensities are high enough that the need for dc light bias is substantially reduced. This finding will be discussed in more detail in a future publication.) The irradiance for each LED and applied current setting was measured by a calibrated spectroradiometer and the centroid emission wavelength was determined by

$$\lambda_c = \frac{\int \lambda . E(\lambda) d\lambda}{\int E(\lambda) d\lambda} \, , \tag{1}$$

where $E(\lambda)$ is the LED's spectral irradiance. It should be noted that an effective emission wavelength [17], which takes into account the shape of the LED spectrum and the responsivity function of the reference detector and the DUT, is a more accurate way of determining the LED's effective wavelength (than the centroid approach). However, since the bandwidths of the devices' spectral response are many times larger than the emission spectra for each of the 33 chosen LEDs, the expected error from this oversimplification is small. Additional details on the operation of the LEDs including the emission peak linewidths, the operation stability in pulsed mode, cold plate temperature effect, etc. can be found elsewhere [10,12,15].

C. System calibrations and cell measurements

In order to perform spectral response measurements of solar cells, first a system calibration is performed. The calibrated spectral irradiance responsivities (the SR of the standard reference detector $R_{s,irrd}(\lambda)$) associated with a NIST reference photodetector [19] is transferred to the monitor Si or Ge detectors. For the data obtained as part of this work, where all the cells tested had responsivities in the range of 300 nm to 1200 nm, the Ge transfer was not needed, and only the Si reference detector was used. In this case, the reference detector is mounted at the measurement plane of both configurations (e.g., tight to the sphere and offset 60 cm) and the LEDs are sequentially swept while the reference cell voltage $V_s(\lambda_c)$ and the monitor detector voltage $V_m(\lambda_c)$ are measured. From this data, the calibration value, $C(\lambda_c)$, is determined using

$$C(\lambda_c) = \frac{R_{s,irrd}^*(\lambda_c)}{2.221 G(V_s(\lambda_c) / V_m(\lambda_c))} \, , \tag{2}$$

where $R_{s,irrd}^*(\lambda_c)$ is the effective SR of the reference detector, subjected to LED illumination and is defined as

$$R^*_{s,irrd}(\lambda_c) = \frac{\int R_{s,irrd}(\lambda).E(\lambda)\mathrm{d}\lambda}{\int E(\lambda)\mathrm{d}\lambda} \ . \tag{3}$$

The gain factor G is defined as $G = G_m / G_{DUT}$, where G_m is the monitor detector's preamplifier gain (typically set at 10^5 V/A) and G_{DUT} is the amplifier's gain for the device undergoing testing. In this case, G_{DUT} was set to the gain setting used when recording the standard detector's output voltage, V_s. The numerical factor 2.221 allows converting root-mean-square (RMS) signal values to peak-to-peak values because lock-ins measure the first Fourier (sine) component of the input signal.

Once the calibration value for the centroid wavelength of each LED is determined, the spectral responsivity of the device undergoing testing in irradiance mode $R_{t,irrd}(\lambda_c)$ is obtained from

$$R_{t,irrd}(\lambda_c) = 2.221C(\lambda_c)G(V_t(\lambda_c)/V_m(\lambda_c)) \tag{4}$$

where $V_t(\lambda)$ is the voltage signal from the cell undergoing testing. $R_{t,irrd}(\lambda_c)$ has SI units of $\mathrm{Am^2W^{-1}}$.

D. Irradiance uniformity

The irradiance uniformity in the test plane of the measurement is important due its effect on the overall measurement uncertainty. The irradiance at the sphere's exit test plane was measured while operating a few different LEDs scattered within the input port's mounted array. In each case, the particular LED was driven in pulsed mode and a photodetector with an area of 1 cm^2 was incrementally moved in 2 cm steps over the entire 15 cm by 15 cm measurement plane. At each location, the signal from the cell was measured by the lock-in amplifier and recorded by the computer. The LED signal was stable to better than 0.05 % within a period of 30 min. Figs. 2(a-d) show the results of this uniformity mapping at the exit port plane for four different LEDs. The percentage nonuniformity is calculated by the formulation $(\max value - value_i) / (\max value + value_i) \times 100$, where the "max *value*" is the largest recorded signal in the measurement plane and "*value$_i$*" is the signal from each of the other locations.

As shown in Fig. 2 for the entire 15 cm × 15 cm mapped area (xy points represent the location of the center of the detector), the nonuniformity is lower than 1.8 % for all four LEDs. For all four of these uniformity checks, large areas, on the order of 8 cm to 10 cm, are created where the percentage non-uniformity is less than 0.5 %. This spatially evaluated illumination is a significant improvement over the lightguide approach reported previously [12]. Fig. 3 maps the nonuniformity over a 16 cm by 16 cm area at the 60 cm offset illumination test plane (refer to configuration 2 of Fig. 1b). Fig. 3 reveals a central spot with a diameter of about 8 cm where the nonuniformity is less than 1 %. For a typical 12.5 cm (≈ 5 in) Si solar cell, as outlined by the dotted square in Fig. 3, the non-uniformity drops to about 3 % near the corners while for larger 15.2 cm (6 in) solar cells, the non-uniformity further drops to 6 % near the corners. This degree of edge tapering is still significantly better than what was achieved using our previous system. Furthermore, due to the bell-shaped (Gaussian) distribution of nonuniformity, the error associated with the nonuniformity for large area cells can be determined relatively easily by making some reasonable assumptions. The measurement uncertainty due to nonuniformity for small area cells (< 5 cm), or for situations where the area of the reference detector is similar to the device undergoing testing – and so both are mounted and measured at a similar location, such as the center of the map – is less than 0.2 %. For

large area cells where the effect of nonuniformity is larger, the median value of the signal in the uniformity map over the area of the cell tested is compared with the signal from the central location where the calibration was performed. A scaling factor, typically on the order of 1.018 for cells up to 15 cm was determined from this comparison and is applied to the SR data recorded from the cell. The uncertainty due to this procedure is estimated to add an additional 0.4 % to the overall uncertainties.

3. Results and Discussion

A. Importance of irradiance spectral response measurements

As reported previously, a cell's irradiance mode SR curve can be determined by first making a complete set of power-mode spectral response measurements – such as done using the monochromator based method (where the beam underfills the cell) -- and then scaling all of the power-mode data based on the results from a single LED irradiance-mode SR measurement. [10]. This approach works fairly well for single crystalline silicon or other material cells (including filtered cells) where the shape of the SR curve does not significantly change from one locally illuminated location to another. The inset in Fig. 4 shows power spectral responsivity R_{pwr} measurements for a single-crystalline Si cell with each curve representing the SR at a different illuminated location across the surface of the cell. In cases like this, the irradiance SR curve can be easily obtained using the approach mentioned above without having to perform more than one or two single LED irradiance-mode measurements for scaling purposes. Using the scaled irradiance-mode SR curve, the I_{sc} of the cell for any defined solar spectrum, including the standard AM 1.5 spectrum, can be determined [10]. For the specific case of AM 1.5 spectrum, the results agree very well with outdoor measurements of the I_{sc} based on World Radiometric Reference (WRR) scale.

Other types of solar cells such as polycrystalline Si cells, however, do show spatially-dependent spectral responsivity curves. This characteristic is shown in the main part of Fig. 4 for a polycrystalline cell, where the differences are particularly significant in the near-IR range closer to the band gap of the material and is likely due to the spatial distribution of defects or quality of the crystalline regions. In this case, obtaining the one curve representing the whole of the device response is not straightforward and may require a local mapping approach and an advanced statistical methodology for deducing the overall device SR curve. In this case, the LED integrating sphere approach described in this paper, with its uniform overfilled illumination and a variety of LED spectra, is the simplest way for obtaining the overall irradiance-mode SR curve of the entire cell. Every LED can be viewed as a local scaling factor for irradiance-mode SR. This inherent feature is further illustrated in the following section.

B. Small-area cell measurements

In Figs. 5(a) through 5(d), the SR data are shown for four types of reference solar cells with dimensions of $\approx$ 2 cm by 2 cm and prepared according to the World Photovoltaic Scale (WPVS) package design (without encapsulation). Data shown in Figs 5(a) and 5(b) are obtained from two mono crystalline Si cells; Fig. 5(c) shows the data from a polycrystalline Si cell, and Fig. 5(d) shows the data for a monocrystalline Si cell with a KG5 window. Two sets of data for each cell, one with the diffuse mode of configuration 1 (Figure 1a) and the other with the semi-collimated mode of configuration 2 (Figure 1b) are shown. Also plotted are the SR curves obtained by the monochromator measurement and scaled by a single LED irradiance-mode data (typically a 538 nm LED). An appropriate level of light bias has been

used in all four cases and for both types of measurements to bring the cells into the linear operating regime. Clearly, the diffuse mode measurements in all but Fig. 5(a) are significantly different from the semi-collimated results. Of the two options, the monochromator with single LED scaling results agree better with the semi-collimated LED measurements. The outcome is expected because the underfilling beam of the monochromator is relatively collimated.

The main reason for the discrepancy between the two types of measurements for cells in Figs. 5(b) through 5(d) is that the directional or cosine responses of these three devices are different from the reference detector used to calibrate the system. This interpretation has been further validated for these cells by performing angular response measurements. The samples were mounted on a goniometer and then subjected to incidence illumination when oriented from normal incidence to as high as 55° off normal. These measurements for two different radiation wavelengths are shown in Figures 6(a) and 6(b). The solar cells that showed the largest deviations from the reference detector's directional response demonstrate the greatest disparity between the diffuse and the semi-collimated measurements. It was also observed that the cosine response is significantly wavelength-dependent. The solar cell whose data was shown in Fig. 5(a), however, has a more closely matched angular response to that of the reference detector; therefore the transfer from the reference detector to the solar cell under diffuse lighting works relatively well although not perfectly.

These LED integrating sphere measurements present a refinement to the hybrid monochromator/single LED approach for determining the irradiance mode SR of cells with material nonuniformity across the cell. For example, the semi-collimated SR data in Fig. 5(c) for the same poly-Si cell of Fig. 4 represents the correct shape of the SR for this cell; the monochromator-based curve in Figure 5(c) is a simple averaged plot for all the measurements presented in Fig. 4 and, as such, does exemplify that multiple curves using the older method are needed to approach the SR curve obtain from using only one set of LED integrating sphere method data. This comparison demonstrates that the multi LED integrating sphere irradiance mode approach is the more accurate way of obtaining the spectral response measurements of solar cells, particularly in cases where the material is nonuniform. Measurements obtained using the LED integrating sphere approach can also be combined with monochromator data to obtain hybrid monochromator/LED spectral response curves with even better wavelength resolution.

C. Directional (cosine) response

The results reported in this paper illustrate that reference cells or detectors calibrated by national labs, including NIST, for the purpose of irradiance measurements should not be deployed under diffuse lighting conditions unless the DUT has a very closely-matched directional response to the reference detector. If that is the case, i.e., transferring the SR from one identical reference diode or solar cell to another, as in cases of rapid volume calibrations, then the integrating sphere source operated in diffuse mode configuration 1 can be used without any major sources of error due to differences in angular response. In other general cases such as those outlined here, however, great care must be taken with regard to angular mismatch. If the capability to measure the wavelength-dependent angular response of a cell does not exist or deemed too tedious of a task, the most innocuous approach to determine the SR curve of a cell is to perform the measurements under a more direct illumination with a projected or collimated source (as opposed to diffuse) presenting a narrower field of view for the DUT.

Furthermore, the SR curves represented by the scaled monochromator-based data which pass through the collimated mode LED measurements correctly predict the I_{sc} of the cell when

subject to an AM 1.5 G spectrum (to better than 1 % uncertainty [10]). This good performance results because the AM 1.5 G spectrum has the majority of its irradiance in direct/collimated incidence (consisting of 88 % direct incidence, 2 % circumsolar and 10 % sky diffuse and ground reflected). This realization, however, brings into question the potential loss of accuracy created by using a reference cell calibrated under normal incident illumination to monitor the irradiance on diffuse cloudy days, or even during tests where a solar simulator having a diffuse-light source is employed. The evaluation of these errors is currently under investigation at NIST and by others [20].

D. Large-area cell measurements

Having first evaluated the described system using common types of small reference solar cells, the next step was to make measurements of large-area reference cells. Figure 7 plots the spectral responsivity of three types of encapsulated reference cells: cell#1, a c-Si product with dimensions of 155 mm × 155 mm, cell#2, a pc-Si product with dimensions of 124 mm × 124 mm, and cell#3, another c-Si product also with dimensions of 124 mm × 124 mm (although with cut corners). It can be seen from the plots that the diffuse and the collimated measurements for each cell agree better for these encapsulated cells, except for the 800 nm to 1000 nm region. For this case, as in the previous cases for small cells, the collimated measurements (filled points) are the ones that represent the true SR curve of these three cells and the diffuse measurements (hollow points) must be corrected for the discrepancy in the > 800 nm region. The solid line through each collimated measurement is constructed via a combination of interpolation from the lowest to the highest LED wavelength and the data from the monochromator-based measurements, particularly below 373 nm. Light bias for these measurements were provided by a set of LEDs with emissions in the range of 870 nm to 970 nm; the light bias current causes photocurrent generation that is approximately 4 % to 6 % of the total cell I_{sc}. For these particular cells, this amount of light bias was sufficient to ensure the cell was operating in the linear regime.

In order to further demonstrate the validity of this approach, the I_{sc} under AM 1.5 G standard reference spectrum for these three cells was calculated, with two of them directly compared to the original National Renewable Energy Lab (NREL) calibration certificate (cells#2 and 3). The calculated I_{sc} for cell#2 is 5.44 A ± 0.076 A as compared to three NREL certified values of 5.325 A, 5.393 A and 5.433 A. The NREL values correspond to three separate testing rigs (with an average of 5.38 A). The calculated I_{sc} for cell#3 is 5.23 A ± 0.07 A as compared to the certification value of 5.1669 A (only one certification sheet was available for this cell). Therefore, the NIST measurements agree well with the calibrations: by 1.1 % for cell#2 and by 1.2 % for cell#3. Both of these percent differences fall within the ±1.4 % (k=2) uncertainty that is associated with the NIST values. For the case of cell#1, an I_{sc} = 8.95 A was calculated, although no direct third party comparison exists for this cell.

E. Measurement uncertainty

The relative combined uncertainty (k=1) of the wavelength-dependent absolute spectral response curves for a typical 2 cm Si cell and a 12.5 cm encapsulated Si cell are shown in Fig. 8 and include a variety of type A (uncertainties associated with repeated measurements) and type B (uncertainties associated with various other sources) uncertainties. The most important ones are the primary reference detector or cell calibration uncertainty of ± 0.24 %, wavelength measurement uncertainties of ± 0.07 %, measurement reproducibility of 0.15 %, irradiance uniformity errors of at least 0.2 % for small area measurements and 0.36 % for large area cells. Standard deviations of raw data were also included in all calculations and were typically less than 0.1 %. Uncertainties due to possible correlations have been ignored and the analysis

also assumes an even distribution of local SR variations due to the intrinsic material nonuniformity for the pc-Si cells. The uncertainty associated with the I_{sc} were evaluated based on the procedure described previously [10]. Further detailed evaluation of factors contributing to measurement uncertainties will be in future work.

4. Conclusions

Absolute differential SR measurements in irradiance mode based on a LED array coupled with an integrating sphere source have been demonstrated. Due to good illumination uniformity at the measurement plane and good temporal stability of the light source, the SR uncertainties for both large and small area cells remain small and the short circuit currents calculated with this approach agree well with secondary measurements based on the WRR scale. Furthermore, our results indicate that when there is a mismatch in angular (directional) response between the reference and the test cell, the degree of light collimation from the source plays an important role in the SR and I_{sc} measurements.

References

1.   "Standard test method for spectral responsivity measurements of photovoltaic devices," ASTM Stand. E1021-12 **12.02**, 502–511 (2012).

2.   J. L. Shay, S. Wagner, R. W. Epworth, K. J. Bachmann, and E. Buehler, "A simple measurement of absolute solar-cell efficiency," J. Appl. Phys. **48**, 4853–4855 (1977).

3.   S. Winter, T. Wittchen, and J. Metzdorf, "Primary reference cell calibration at the PTB based on an improved DSR facility," Proc. 16th Eur. Photovolt. Sol. Energy Conf. 1–4 (2000).

4.   J. Metzdorf, "Calibration of solar cells. 1: The differential spectral responsivity method.," Appl. Opt. **26**, 1701–1708 (1987).

5.   R. Ciocan, Z. Li, D. Han, D. Assalone, F. Yang, T. Bilir, E. Ciocan, and K. Emery, "A fully automated system for local spectral characterization of photovoltaic structures," PVSC **35th IEEE**, 1675–1677 (2010).

6.   K. Emery, "Photovoltaic Efficiency Measurements," Proc. SPIE **5520**, 36–44 (2004).

7.   J. S. Hartman and M. A. Lind, "Spectral response measurements for solar cells," Sol. Cells **7**, 147–157 (1982).

8.   J. Metzdorf, S. Winter, and T. Wittchen, "Radiometry in photovoltaics: calibration of reference solar cells and evaluation of reference values," Metrologia **37**, 573–578 (2000).

9.   G. Xu and X. Huang, "Primary Calibration of Solar Photovoltaic Cells At the National Metrology Centre of Singapore," Energy Procedia **25**, 70–75 (2012).

10.   B. H. Hamadani, J. Roller, B. Dougherty, F. Persaud, and H. W. Yoon, "Absolute spectral responsivity measurements of solar cells by a hybrid optical technique.," Appl. Opt. **52**, 5184–93 (2013).

11.   F. C. Krebs, K. O. Sylvester-Hvid, and M. Jørgensen, "A self-calibrating led-based solar test platform," Prog. Photovolt Res. Appl. **19**, 97–112 (2011).

12.   B. H. Hamadani, J. Roller, B. Dougherty, and H. W. Yoon, "Versatile light-emitting-diode-based spectral response measurement system for photovoltaic device characterization.," Appl. Opt. **51**, 4469–76 (2012).

13. G. Zaid, S.-N. Park, S. Park, and D.-H. Lee, "Differential spectral responsivity measurement of photovoltaic detectors with a light-emitting-diode-based integrating sphere source.," Appl. Opt. **49**, 6772–83 (2010).

14. D. L. Young, B. Egaas, S. Pinegar, and P. Stradins, "A new real-time quantum efficiency measurement system," PVSC **33rd IEEE**, 1–3 (2008).

15. B. H. Hamadani, K. Chua, J. Roller, M. J. Bennahmias, B. Campbell, H. W. Yoon, and B. Dougherty, "Towards realization of a large-area light-emitting diode-based solar simulator," Prog. Photovolt Res. Appl. **21**, 779–789 (2013).

16. M. Bliss, T. R. Betts, and R. Gottschalg, "An LED-based photovoltaic measurement system with variable spectrum and flash speed," Sol. Eng. Mater. Sol. Cells **93**, 825–830 (2009).

17. J.-M. Hirvonen, T. Poikonen, A. Vaskuri, P. Kärhä, and E. Ikonen, "Spectrally adjustable quasi-monochromatic radiance source based on LEDs and its application for measuring spectral responsivity of a luminance meter," Meas. Sci. Technol. **24**, 115201 (2013).

18. I. Moreno, J. Muñoz, and R. Ivanov, "Uniform illumination of distant targets using a spherical light-emitting diode array," Opt. Eng. **46**, 033001 (2007).

19. T. C. Larason and J. M. Houston, "Spectroradiometric detector measurements: ultraviolet, visible, and near-infrared detectors for spectral power," NIST Spec. Publ. **250-41**, (2008).

20. S. Winter, D. Friedrich, and T. Gerloff, "Effect of the angle dependence of solar cells on the results of indoor and outdoor calibrations," proceeding 25th EU-PVSEC 4304 – 4306 (2010).

Figure Captions

Figure 1: (a) Overview of the LED-based integrating sphere-coupled spectral response measurement system. A solar cell with dimensions of up to 16 cm is mounted at the exit port of the sphere and is sequentially exposed to simultaneous modulated monochromatic LED illumination and stable dc light bias. (b) In this mode, collimating lens optics projects the light onto the DUT at distance farther away from the sphere. Light bias is provided by various dc operated LED light sources mounted on both sides of the cell. All other aspects of the sphere remain the same.

Figure 2: Illumination uniformity maps at the plane of the exit port produced by 4 of the back-plate LEDs. The LEDs wavelengths are: (a) 467 nm (b) 652 nm (c) 691 nm (d) 1063 nm. The detector used for this mapping has an aperture area of 1 cm^2.

Figure 3: Illumination uniformity map at the location of configuration 2 (see Fig. 1b), produced by a pulsed 516 nm LED. The dashed square represents the size and location of a 12.5 cm reference solar cell mounted at this measurement plane.

Figure 4: (inset) Power-mode spectral response curves for a large monocrystalline Si solar cell measured at a variety of locations across the cell. (main) A series of power SR curves for a polycrystalline cell at different locations across the cell. For all cases, the probing beam diameter was about 1 mm.

Figure 5: SR curves in irradiance mode for a few select 2 cm by 2 cm solar cells by using both the collimated and the diffuse illumination mode. The differences between the two measurements for each cell are attributable to differences in the angular response between the reference cell and the test cell.
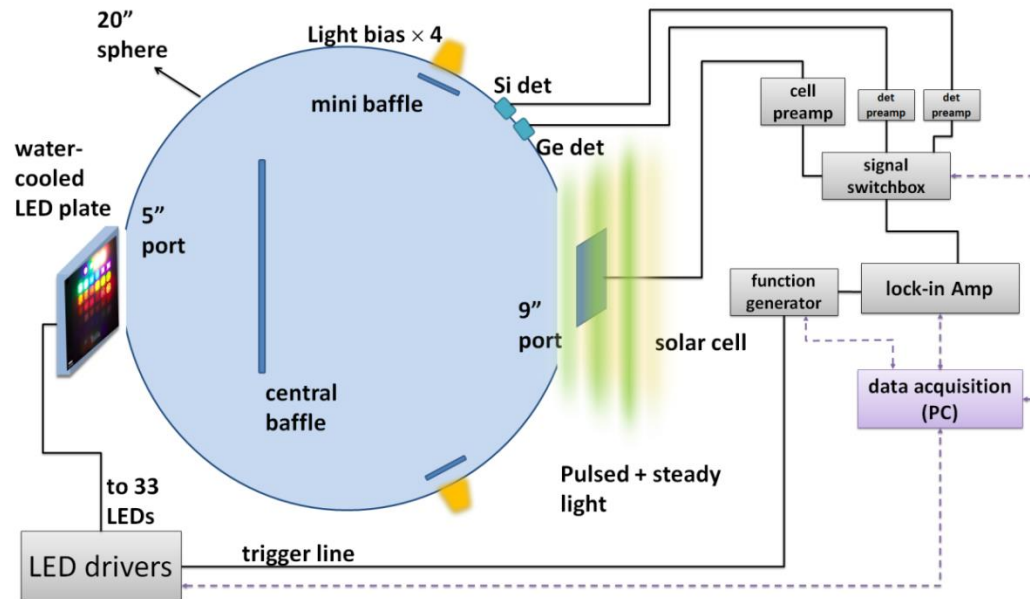
Figure 6: Measurements of the directional response (cosine response) of a few variety of packaged reference cells and detectors at two different wavelengths as marked on the graphs.

Figure 7: SR curves in irradiance mode for 3 types of encapsulated reference cells: cell#1 a c-Si product with dimensions of 155 mm × 155 mm, cell#2, a pc-Si product with dimensions 124 mm × 124 mm, and cell#3, another c-Si product also with dimensions of 124 mm × 124 mm (although with cut corners).

Figure 8: Relative combined k = 1 standard uncertainty of the LED-based spectral response measurements for a 2 cm and a 12.5 cm silicon solar cell.

Figure 1

(a)

20" sphere

Light bias × 4

Si det

mini baffle

Ge det

water-cooled LED plate

5" port

9" port

solar cell

cell preamp

det preamp

det preamp

signal switchbox

function generator

lock-in Amp

central baffle

Pulsed + steady light

data acquisition (PC)

to 33 LEDs

LED drivers

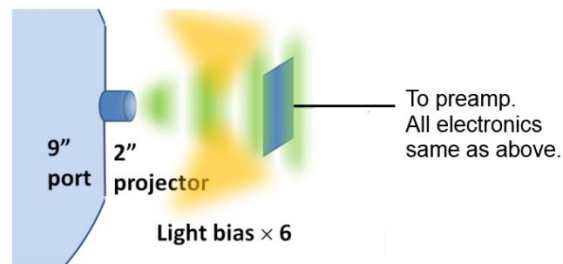trigger line
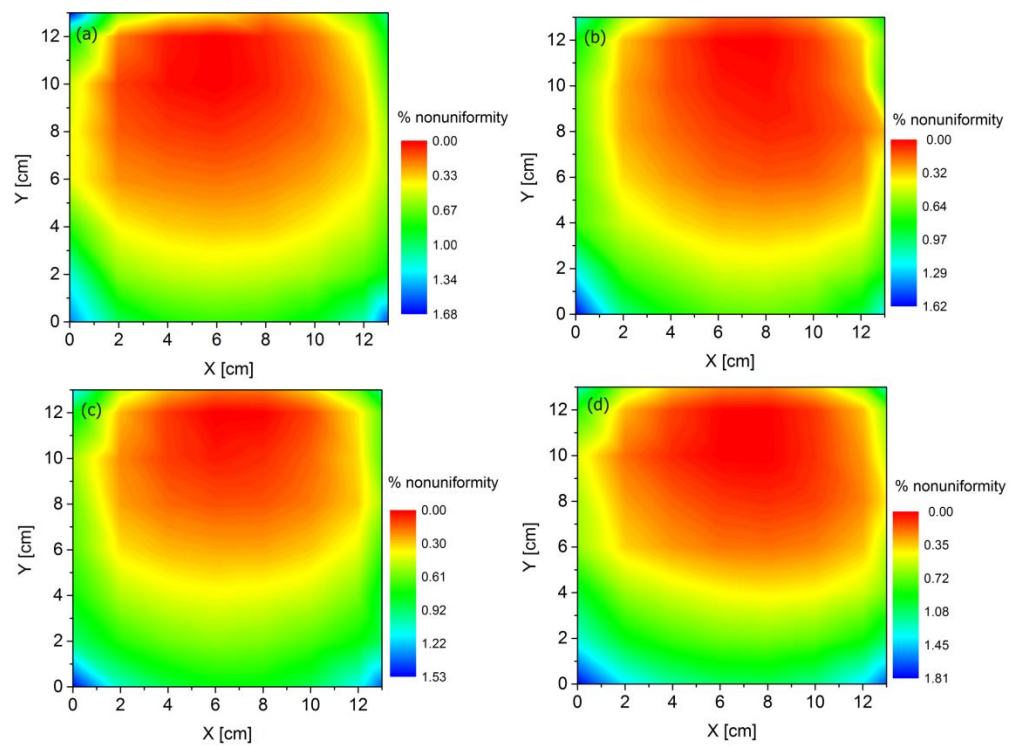
(b)

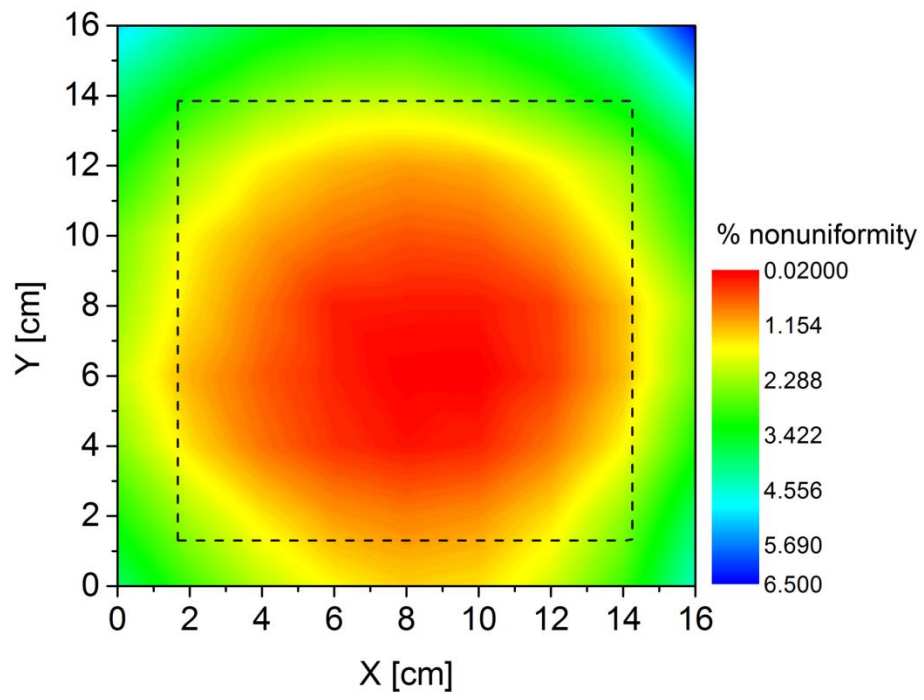9" port

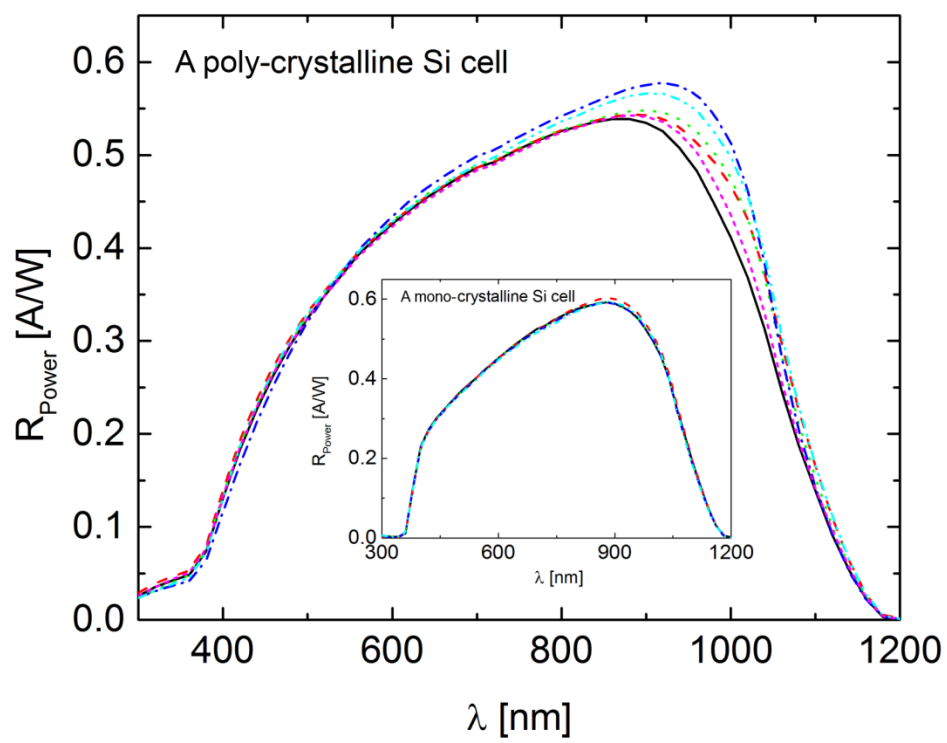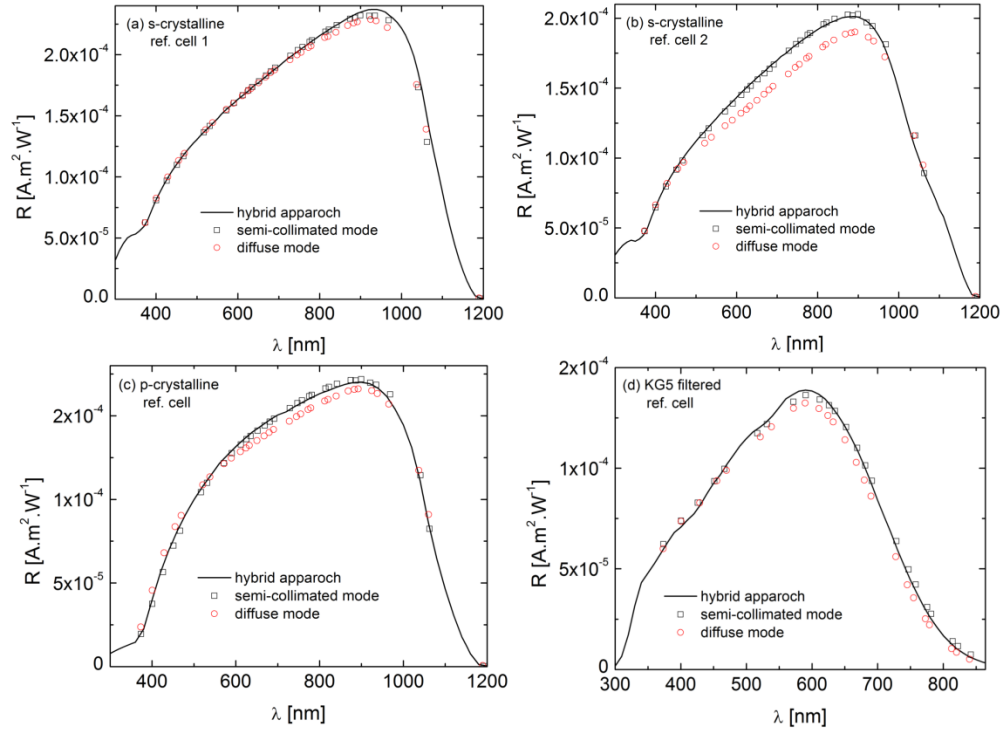2" projector

Light bias × 6

To preamp. All electronics same as above.

Figure 2

Figure 3

Figure 4

Figure 5

Figure 6

Figure 7

Figure 8